Effect of Lower-energy Source on the Tumor Representation in Neutron Stimulated Emission Computed Tomography: An Evaluation Study

by

Yixiao Du

Graduate Program in Medical Physics
Duke Kunshan University and Duke University

Date:_____

Approved:

_____
Anuj Kapadia, Supervisor

_____
James Bowsher

_____
Robert Reiman

Thesis submitted in partial fulfillment of
the requirements for the degree of
Master of Science in the Medical Physics Program
Duke Kunshan University and Duke University

2017

ABSTRACT

Effect of Lower-energy Source on the Tumor Representation in Neutron Stimulated

Emission Computed Tomography: An Evaluation Study

by

Yixiao Du

Graduate Program in Medical Physics
Duke Kunshan University and Duke University

Date:_____
Approved:

_____
Anuj Kapadia, Supervisor

_____
James Bowsher

_____
Robert Reiman

An abstract of a thesis submitted in partial
fulfillment of the requirements for the degree of
Master of Science in the Medical Physics Program
Duke Kunshan University and Duke University

2017

Abstract

Proposed is an investigation into the effect of lower-energy source on the tumor representation of an image acquired by a neutron-based spectroscopic imaging modality, Neutron Stimulated Emission Computed Tomography (NSECT).

The NSECT experiments were performed at a shielded neutron source of the Triangle Universities Nuclear Laboratory (TUNL), which was proficient at creating neutron beams of energy up to 20MeV. However, this neutron generator is not feasible for clinical use due to its large size. Smaller compact sources such as deuterium-deuterium (DD) neutron generators are attractive alternatives that can produce neutrons of sufficient energy to stimulate isotopes of interest in the human body. However, DD generator is not competent at producing neutrons of high energy. Thus, the focus of this work is to evaluate the effect of lower-energy neutrons, such as 2.5MeV and 3.2MeV, on the NSECT images.

The experiments were modeled and simulated in this work using a Monte Carlo toolkit, Geant4. In Geant4 space, an anthropomorphic phantom of cancerous tissue was scanned by a simulated neutron source. During scanning, the phantom was translated to cover the whole field of view (FOV) and rotated over 180 degrees for the purpose of tomographic imaging. Neutrons and gammas emitted were captured by a virtual detector, which could identify the energy and position of each particle. Information of

position and energy of gammas detected resulted in a sinogram for an array of energies, created by selecting the energy characteristic to a specific element. Using the sinograms, two-dimensional maps of the spatial concentration of the element could be reconstructed through a reconstruction algorithm and the elemental concentration revealed the internal geometry of the phantom.

Images were generated when the phantom was scanned by 5MeV, 3.2MeV and 2.5MeV neutron sources. Comparison of tumor parameters in these images indicates that a neutron source of lower energy could degrade the tumor representation in a NSECT image on the aspects of concentration, brightness and underestimation of the tumor size. Then further investigations with 50,000, 100,000, 150,000 and 200,000 neutron events were performed respectively in the 3.2MeV-source case and 2.5MeV-source case in order to test whether the number of neutrons is correlated to the quality of the reconstructed images. Improvement of tumor representation, for example, a clearer tumor region and more accurate tumor size information, shows that increase in the number of incident neutrons has a positive effect on the reconstructed image. This work demonstrates the effect that low energy neutrons have on the image and verifies the feasibility of using low-energy neutrons as the source in NSECT breast imaging.

Table of Contents

List of Tables

List of Figures

Acknowledgements

I would like to thank Dr. Anuj Kapadia for being an outstanding advisor, from whom I learnt so much, not only limited to this thesis project but about how to be a qualified researcher as well. Furthermore, I wish to express my gratitude to all the faculty and staff in Medical Physics program of Duke Kunshan University, for creating such great opportunities and getting us into this field.

1. Introduction

Neutron Stimulated Emission Tomography (NSECT) has been proposed as an in vivo imaging technique with the ability to detect and diagnose cancer through quantifying the concentration of elements in the human body. This is theoretically a revolutionary imaging method that can be implemented in clinics based on the fact that some elements, such as cobalt and sodium, distribute differently between healthy tissue and cancerous tissue. This difference in elemental concentration may be seen prior to the formation of a physical tumor, thus, it enables NSECT the potential of detecting and diagnosing malignancy at an early, treatable stage (Kapadia et al. 2008).

1.1 Elemental Concentration Variation vs. Cancer Diagnosis

Currently, there is evidence available in support of the relationship between the concentration of some trace elements, such as calcium, iron, copper, bromine and zinc, and breast cancer risk. Therefore, these elements can be utilized as tumor biomarkers and any variation on their concentration could be a valid prognostic factor for breast cancer detection (Silva et al. 2012).

Moreover, it has been proven in previous work that NSECT has the ability to detect and identify malignant tissue due to its sensitivity in quantifying minor changes of elemental concentration (Bender et al. 2007).

1.2 Physics Principle of NSECT

The NSECT imaging system utilizes a neutron beam of sufficient energy to stimulate stable isotopes in a sample to excited states, which will immediately drop to the ground state. The decaying process results in the release of energy in the form of gamma ray emissions that will be captured by a gamma spectrometer. Since the energy of these gammas equal to the energy difference between the excited state and the ground state, is characteristic to an individual isotope, we can generate a sinogram for a spectrum of energies and select the energy peak according to the trace element of interest. The system manages to map spatial distribution of the element using a reconstruction algorithm. Any abnormal variation in elemental composition can be seen from the reconstructed image; thus, unhealthiness related to this variation can be detected in this way (Floyd et al. 2006).

Exposure under the neutron source usually takes a few milliseconds per image, if taking patient setup time into account, a neutron scan by NSECT can be performed within several minutes.

1.3 Effect of Neutron Energy on the Image

The spectral information used in the NSECT image reconstruction process is obtained from the interactions between source particles and isotopes in the patient body, mainly inelastic neutron scattering. The probability of occurrence of the neutron

interacting with a nucleus, which is expressed by microscopic cross section, is primarily dependent on the energy of the incident neutron for a given target. Commonly, neutrons at lower energies are more likely to interact with matter than those at high energies because of their slower travelling speed, which favors the data acquisition in NSECT. However, considering that lower source energy could potentially limit the number of gammas emitted, which is correlated with the brightness of tumor region on the image, a neutron source of properly high energy is required for the sake of strong signal.

The macroscopic cross section, which means the probability of a given reaction occurring per unit travel of the neutron, can be calculated as the product of the microscopic cross section and atomic density of the material. A compressed tissue has a higher atomic density, leading to a larger macroscopic cross section. But the increase in this probability does not necessarily contribute to the neutron interaction of interest in NSECT imaging, and more neutron interactions irrelevant to image reconstruction could add to background noise.

From the above, NSECT imaging behavior determined by neutron inelastic scattering is closely related to the microscopic neutron cross section, therefore, the energy of neutron source utilized in NSECT has an influence on the tumor representation of images, and our aim is to evaluate the effect of source energy. In the

present work, neutron source of 5MeV is chosen to be a contrast for its competence to provide best display of the tumor.

Previously, the NSECT system used a Van-de-Graff accelerator that can provide high-energy neutrons for stimulating abundant isotopes in the human body. However, practical issues, such as safety features and the need for an appropriate size of the equipment in hospital rooms make Van-de-Graff accelerator not suited to be a clinically achievable imaging system because of its size, substantial cost and complexity of operation. Neutron Generators (NG) appear to be a better option on the grounds that they could yield a high flux of up to 10^{10} neutrons out of a compact size device. NGs are based on either deuterium-deuterium (DD) reactions or deuterium-tritium (DT) reactions. We tend to choose DD generator over DT generator for the reason that tritium is a radioactive gas, so DT generator contains radioactivity even when it is turned off. However, deuterium is not radioactive, which makes DD generator an inherently safer source. Since DD generator produces neutrons of energy 2.5 MeV or 3.2 MeV (in a special situation that 1 MeV deuterons are incident at angle 90 degree), 3.2 MeV and 2.5 MeV sources were investigated in this work. The results and conclusion can be a good reference to select the neutron energy and even determine other setup for future NSECT researchers.

2. Methods

2.1 Anthropomorphic Phantom

A 400mm*400mm*400mm voxelized XCAT phantom (Segars et al. 2010) containing voxels of length 1mm on each dimension was used as a realistic representation of tumor in the vacuum. A 3D display of the phantom and the coronal plane of this phantom scanned in our simulation are shown in the figures below.

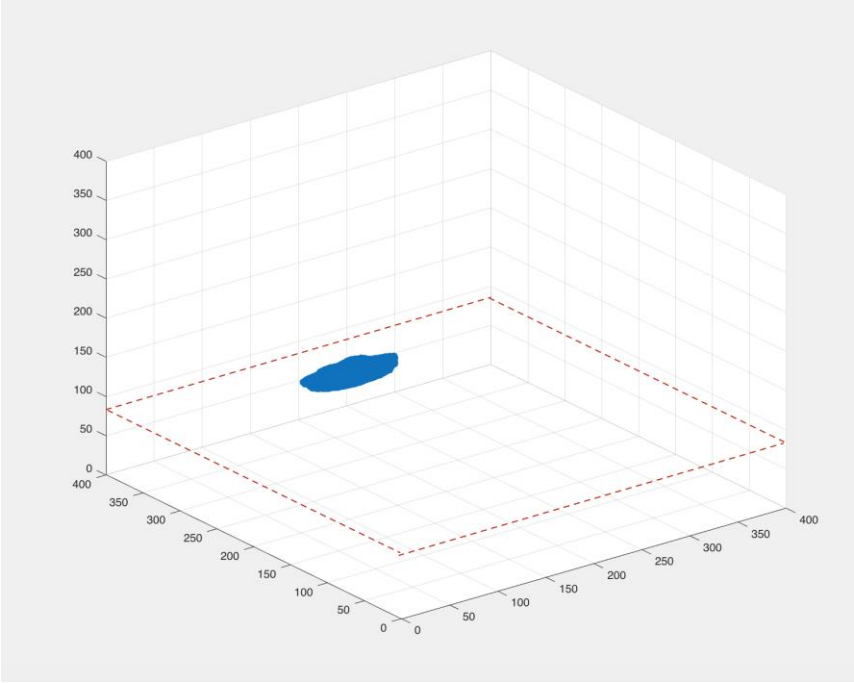

Figure 1: 3D display of the phantom. Blue object: tumor.

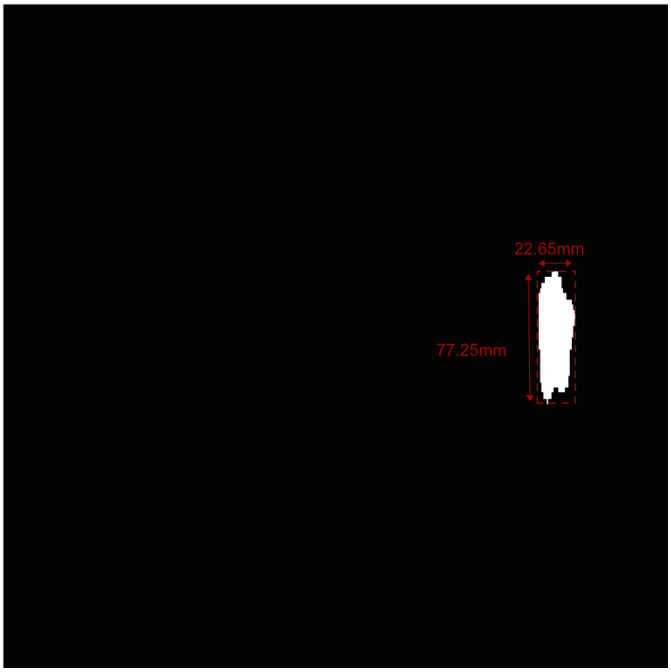

Figure 2: Coronal plane of the anthropomorphic phantom. White part: tumor; black part: environment of vacuum. Red text: actual tumor size(77.25mm*22.65mm).

Some voxels in the phantom were assigned with various elemental compositions to mimic the malignant area and others were filled with nothing to represent the vacuum environment. The elemental concentrations were decided according to earlier studies by Bender et al. (2007) and are shown in Table 1.

Table 1: Elemental concentrations in malignant area(Bender et al. (2007))

	Malignant(%)
H	12.51
O	61.43
C	22.86
N	2.57
Al	5.7E-4
Br	6.55E-4
Ca	1.13E-2

Cl	2.15E-1
Co	1.98E-5
Cs	3.6E-7
Fe	7.85E-3
K	1.96E-1
Mn	3.16E-5
Na	2.0E-2
Rb	5.84E-4
Zn	1.14E-3

2.2 Software Package for Data Acquisition---Geant4

Since the project needs a large amount of simulations, but operating on the real NSECT system for every simulation will cost too much on the time, finances and human efforts, it is impractical to conduct experiments on a real NSECT imaging system, thus, all the data needed for image reconstruction in this study were simulated by a Monte Carlo toolkit, Geant4.10.2. Geant4 was created for relatively accurate simulations of a comprehensive range of physics processes occurring during particle interactions with matter (Agostinelli et al. 2003).

In this project, we set up the simulation geometry in the model that contained a Geant4 world. A voxelized phantom was positioned at the center and neutron particles were shot from a point outside the phantom on the chosen plane. In a clinical situation, we are supposed to rotate the source beam around the phantom for obtaining a tomographic image but in this model, for convenience, we rotated and translated the phantom instead of the source. Based on the previous experience in NSECT imaging, 50,000 neutrons is a good start to generate reasonable images. Thus, at first, we ran

50,000 neutron histories and performed three sets of simulations with 5 MeV, 3.2 MeV and 2.5 MeV source beams respectively. During the scanning process, the phantom was rotated 15 times over 180 degree and for each rotation, it was translated by 52 or 56 stops for complete scan.

The field of view (FOV) was set as 56 centimeters to fully cover the 40cm-side phantom even when it moved to a diagonal position to source direction (Figure 2).

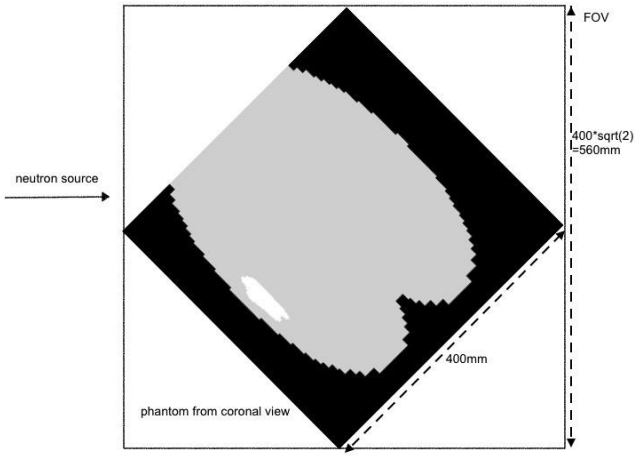

Figure 3: Display of FOV and the phantom at the diagonal position

Since beam width and the spatial increment define the smallest dimension that can be resolved, they should be small enough to avoid missing any lesion (Raterman 2013). For fully cover the FOV, the translational increment is determined by dividing FOV(56cm) by the most phantom translations used in this project, i.e. 56 translations. Thus, the beam width was set to be the same as the numerical value of translational increment, i.e. 1cm.

2.3 Image Reconstruction

The data acquired from Geant4 was a spatial map of gammas, and from information about the numbers of the emitted gammas of s sequence of energies, the location of a particular neutron scattering event can be detected by applying an image reconstruction method to the sinogram corresponding to the chosen element, called the Maximum Likelihood Expectation Maximization (MLEM) method. This is an iterative method that is widely acknowledged to be one of the best for image reconstruction.

The energy selected for reconstruction is the prominent peak energy in the obtained gamma energy spectrum. The figure 3 is an example of how we chose 440keV in the 2.5 MeV-source simulations, it can be seen obviously in the figure below that 440keV is distinguished from the spectrum.

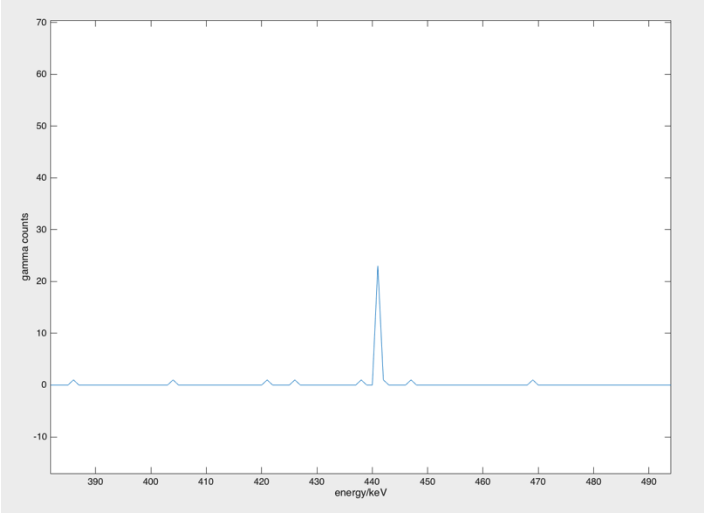

Figure 4: The peak of energy 440keV on the gamma spectrum from one of the simulations.

By this way, it was decided that the following energies of the gammas characteristic to the element were appropriate for reconstructing images,

1). 5MeV: 440keV(Na), 1636keV(Na), 2313keV(N), 4439keV(C);

2). 3.2MeV: 440keV(Na), 1038keV(Fe), 1636keV(Na), 2313keV(N), 2391keV(Na);

3). 2.5MeV: 440keV(Na), 1636keV(Na).

2.4 Evaluation Parameters

Two parameters were measured in each image,

1). Average intensity and fractional standard deviation in the tumor region of images

2). Full-width at half-maximum (FWHM) of tumor region in image

The average intensity is correlated to the brightness of tumor area in the images generated by simulation data, and a smaller standard deviation leads to better tumor representation with less noise caused by neutron interacting with matter other than tumor in patient body. Since variations due to the background noise were taken into account this way, FWHM here can be a convincing estimation of the size of tumor. The purpose of measuring these two parameters was to assess the performance of tumor representation in the reconstructed images, which is significant to the diagnostic confidence of NSECT.

3. Reconstructed Images

The following images were generated from simulations with sources of energy 5MeV, 3.2MeV and 2.5MeV. And the images on the right (acquired with 56 rotations) have a slight superiority in tumor representation than those on the left (acquired with 52 rotations).

3.1 Simulation 1: 5MeV Source

The simulations of a 5MeV neutron source were all run using 50,000 neutron histories.

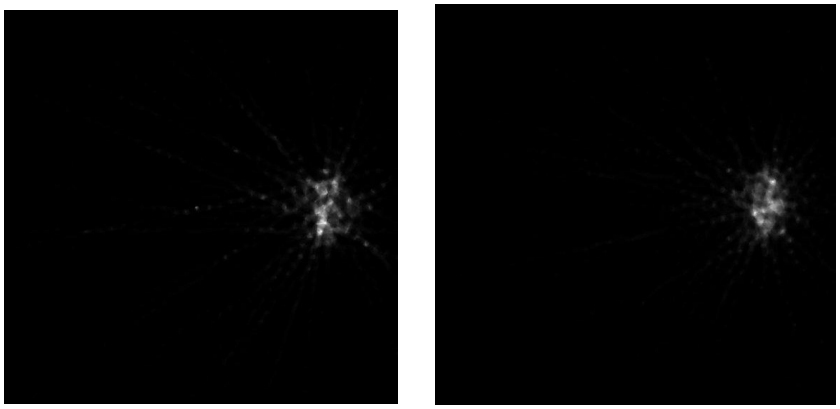

Figure 5: Images reconstructed with energy 440keV. Images on the left were acquired with 52 rotations; images on the right were acquired with 56 rotations.

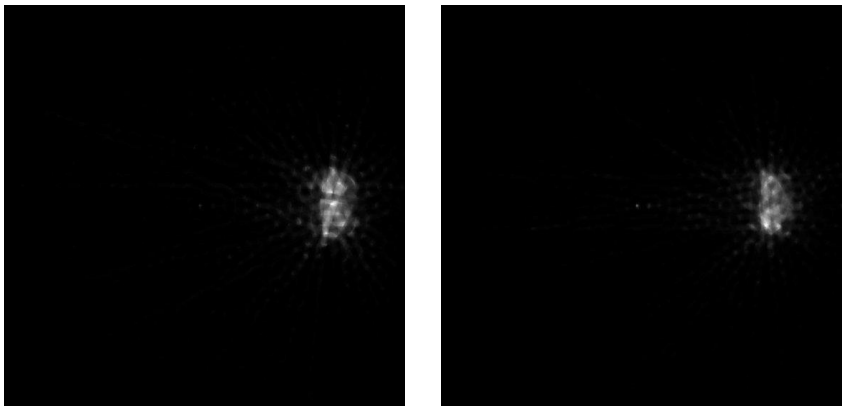

Figure 6: Images reconstructed with energy 1636keV. Images on the left were acquired with 52 rotations; images on the right were acquired with 56 rotations.

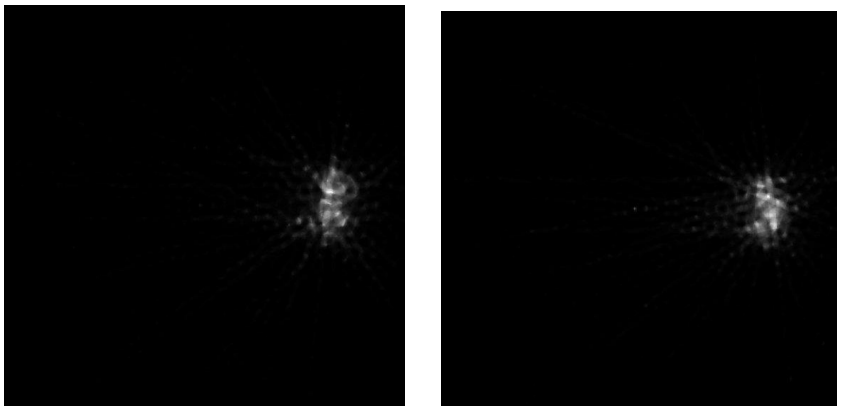

Figure 7: Images reconstructed with energy 2313keV. Images on the left were acquired with 52 rotations; images on the right were acquired with 56 rotations.

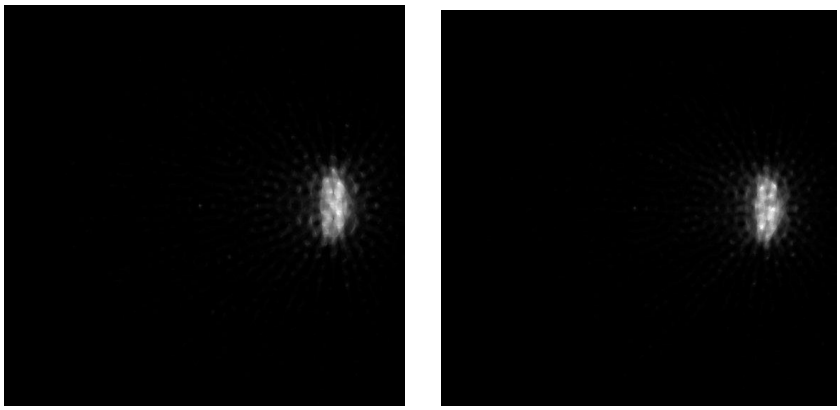

Figure 8: Images reconstructed with energy 4439keV. Images on the left were acquired with 52 rotations; images on the right were acquired with 56 rotations.

3.2 Simulation 2: 3.2MeV Source

3.2.1 50,000 neutron histories

The simulations in the following section were run using 50,000 neutron histories.

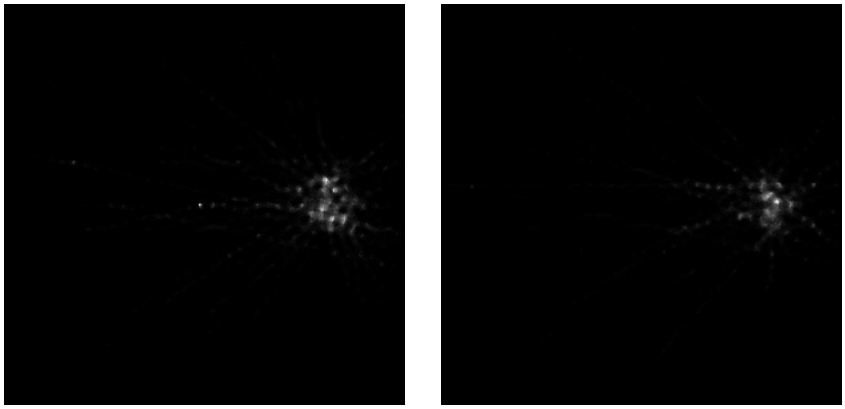

Figure 9: Images reconstructed with energy 440keV. Images on the left were acquired with 52 rotations; images on the right were acquired with 56 rotations.

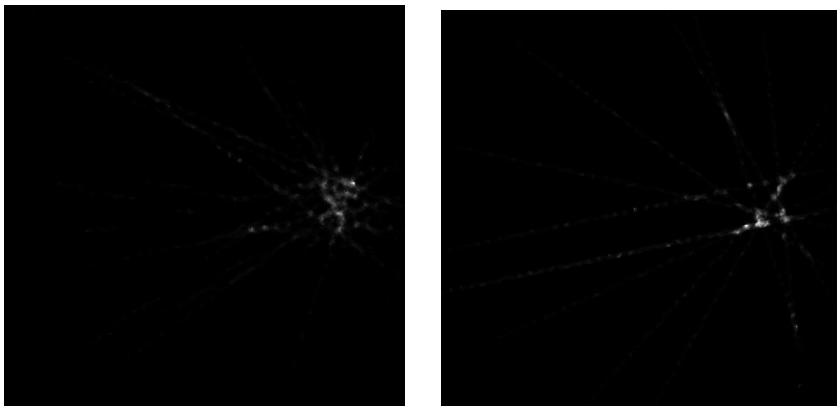

Figure 10: Images reconstructed with energy 1038keV. Images on the left were acquired with 52 rotations; images on the right were acquired with 56 rotations.

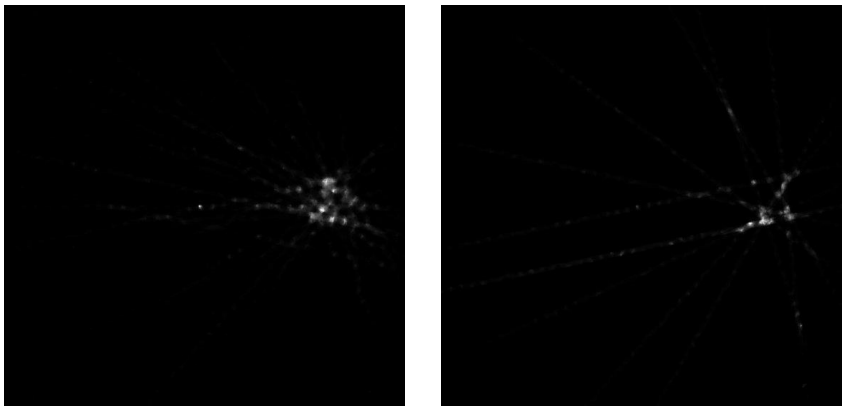

Figure 11: Images reconstructed with energy 1636keV. Images on the left were acquired with 52 rotations; images on the right were acquired with 56 rotations.

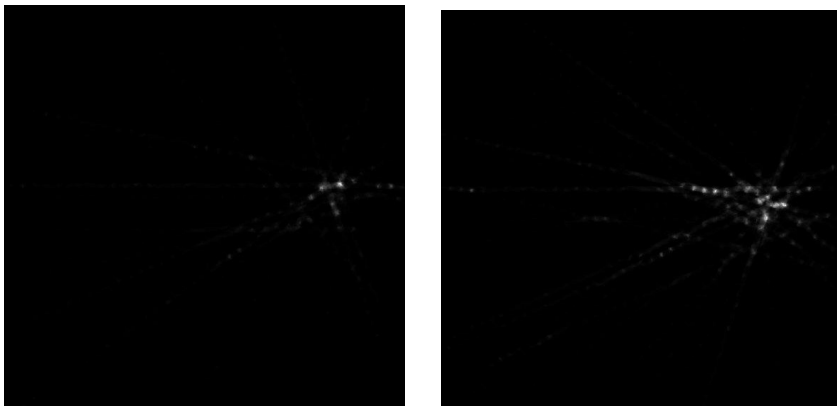

Figure 12: Images reconstructed with energy 2313keV. Images on the left were acquired with 52 rotations; images on the right were acquired with 56 rotations.

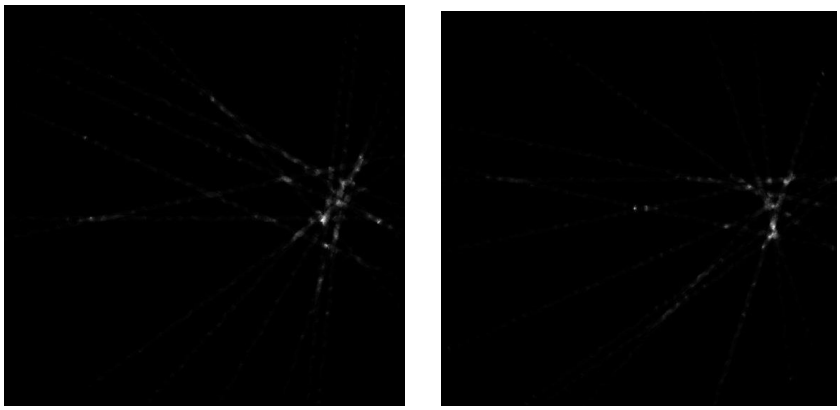

Figure 13: Images reconstructed with energy 2391keV. Images on the left were acquired with 52 rotations; images on the right were acquired with 56 rotations.

3.2.2 100,000 neutron histories

The simulations in the following section were run using 100,000 neutron histories.

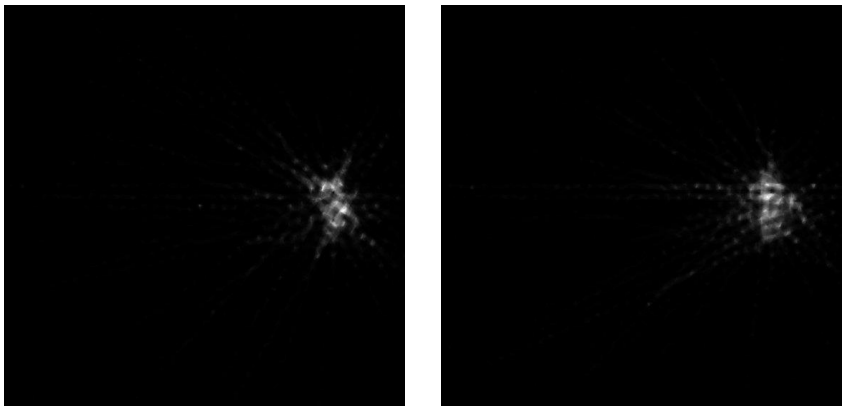

Figure 14: Images reconstructed with energy 440keV. Images on the left were acquired with 52 rotations; images on the right were acquired with 56 rotations.

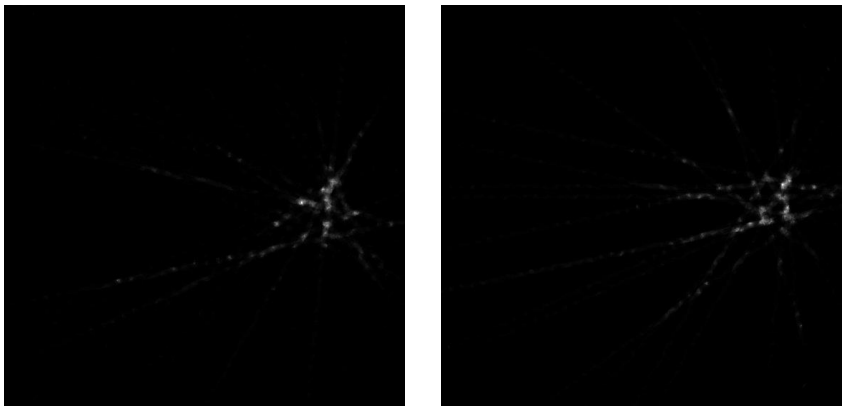

Figure 15: Images reconstructed with energy 1038keV. Images on the left were acquired with 52 rotations; images on the right were acquired with 56 rotations.

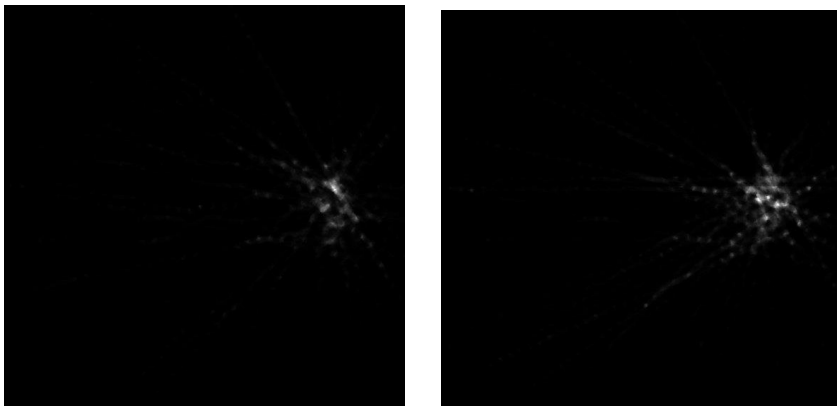

Figure 16: Images reconstructed with energy 1636keV. Images on the left were acquired with 52 rotations; images on the right were acquired with 56 rotations.

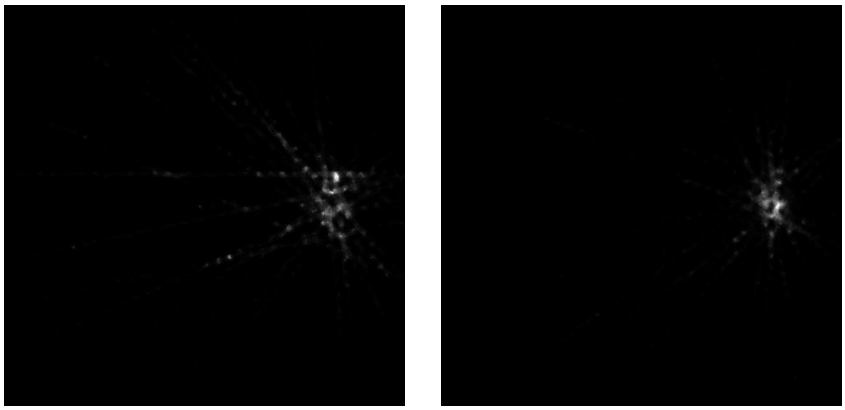

Figure 17: Images reconstructed with energy 2313keV. Images on the left were acquired with 52 rotations; images on the right were acquired with 56 rotations.

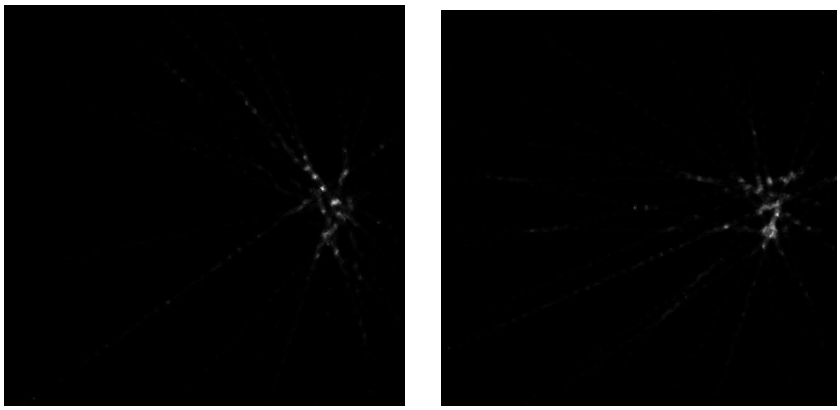

Figure 18: Images reconstructed with energy 2391keV. Images on the left were acquired with 52 rotations; images on the right were acquired with 56 rotations.

3.2.3 150,000 neutron histories

The simulations in the following section were run using 150,000 neutron histories.

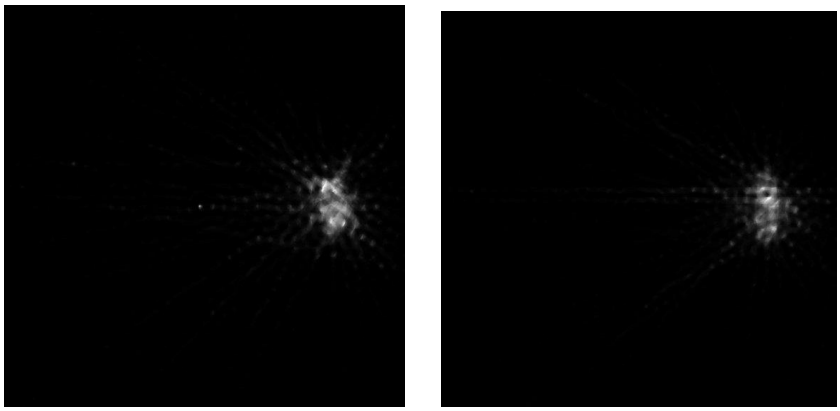

Figure 19: Images reconstructed with energy 440keV. Images on the left were acquired with 52 rotations; images on the right were acquired with 56 rotations.

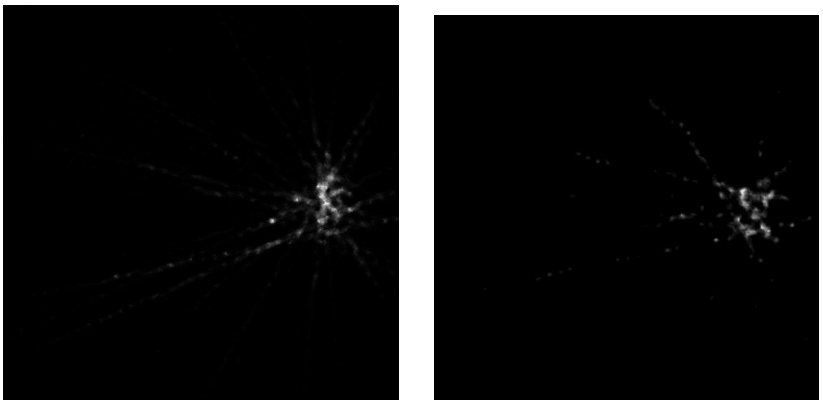

Figure 20: Images reconstructed with energy 1038keV. Images on the left were acquired with 52 rotations; images on the right were acquired with 56 rotations.

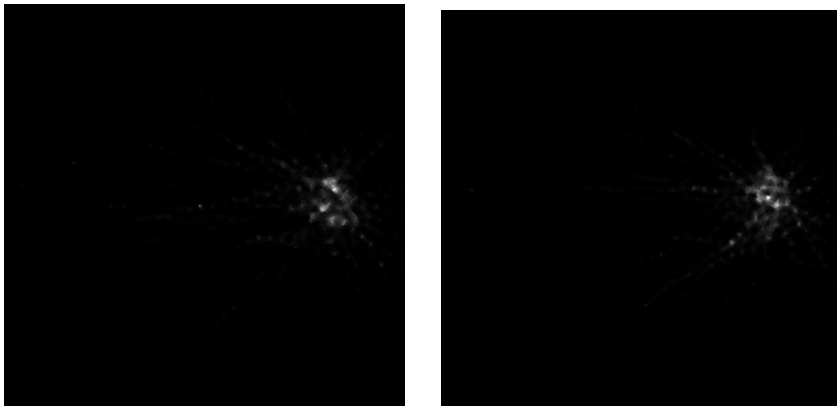

Figure 21: Images reconstructed with energy 1636keV. Images on the left were acquired with 52 rotations; images on the right were acquired with 56 rotations.

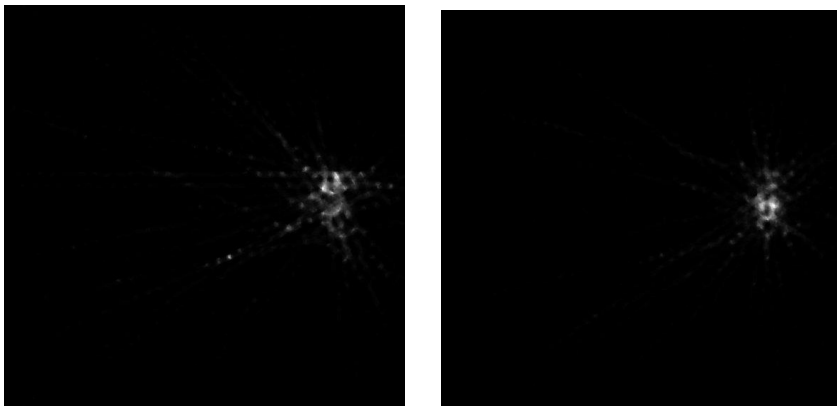

Figure 22: Images reconstructed with energy 2313keV. Images on the left were acquired with 52 rotations; images on the right were acquired with 56 rotations.

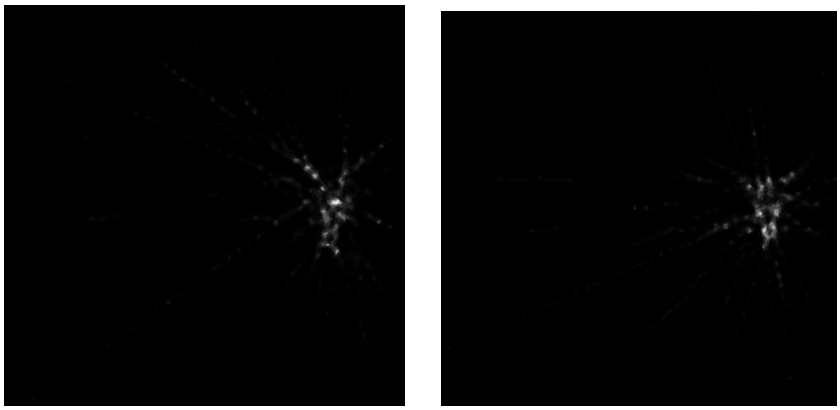

Figure 23: Images reconstructed with energy 2391keV. Images on the left were acquired with 52 rotations; images on the right were acquired with 56 rotations.

3.2.4 200,000 neutron histories

The simulations in the following section were run using 200,000 neutron histories.

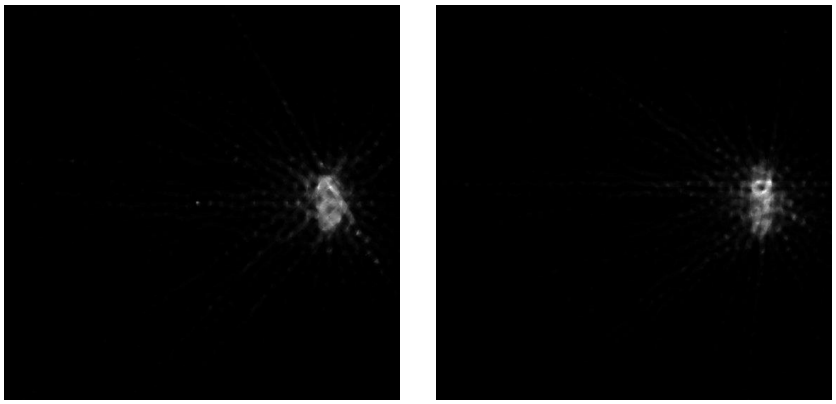

Figure 24: Images reconstructed with energy 440keV. Images on the left were acquired with 52 rotations; images on the right were acquired with 56 rotations.

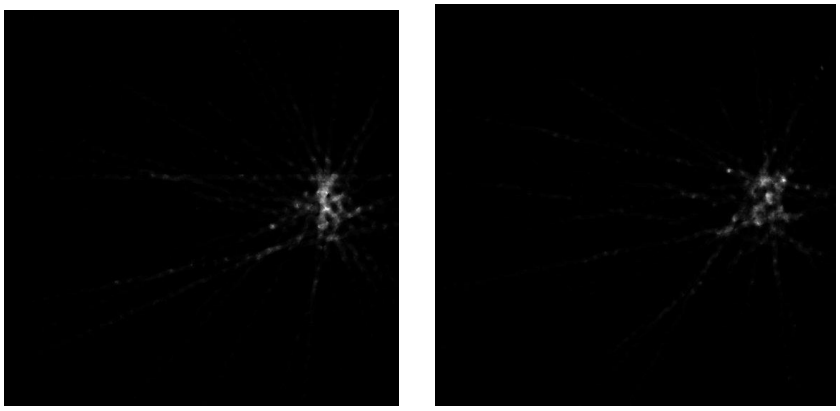

Figure 25: Images reconstructed with energy 1038keV. Images on the left were acquired with 52 rotations; images on the right were acquired with 56 rotations.

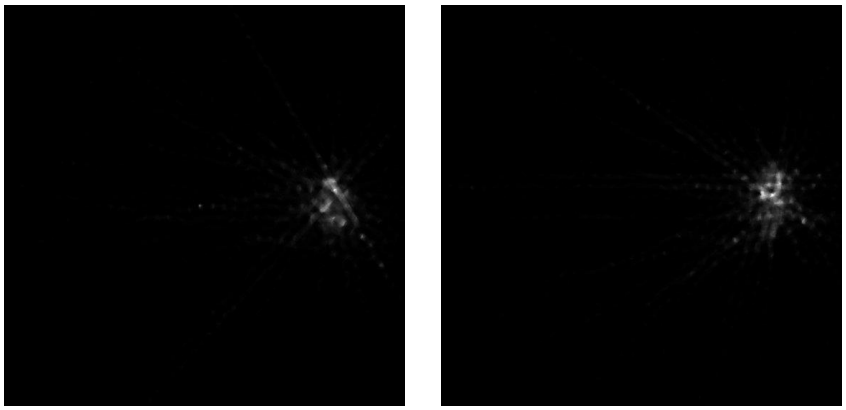

Figure 26: Images reconstructed with energy 1636keV. Images on the left were acquired with 52 rotations; images on the right were acquired with 56 rotations.

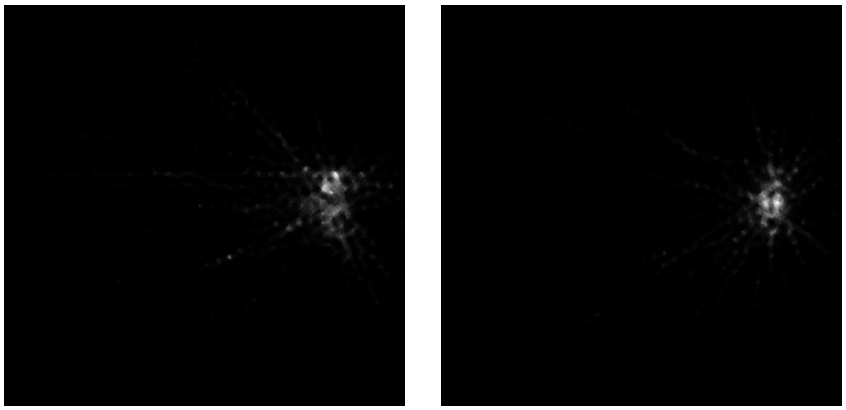

Figure 27: Images reconstructed with energy 2313keV. Images on the left were acquired with 52 rotations; images on the right were acquired with 56 rotations.

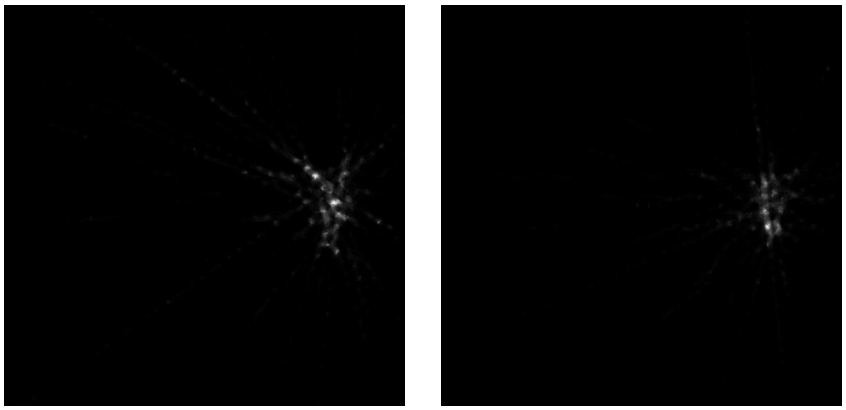

Figure 28: Images reconstructed with energy 2391keV. Images on the left were acquired with 52 rotations; images on the right were acquired with 56 rotations.

3.3 Simulation 3: 2.5MeV Source

3.3.1 50,000 neutron histories

The simulations in the following section were run using 50,000 neutron histories.

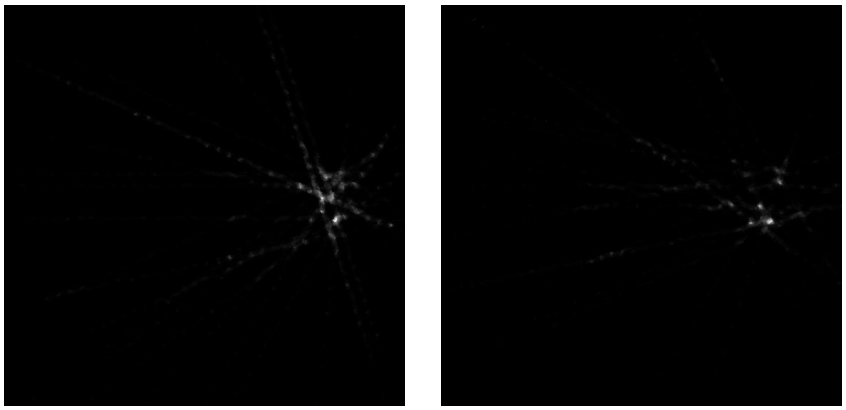

Figure 29: Images reconstructed with energy 440keV. Images on the left were acquired with 52 rotations; images on the right were acquired with 56 rotations.

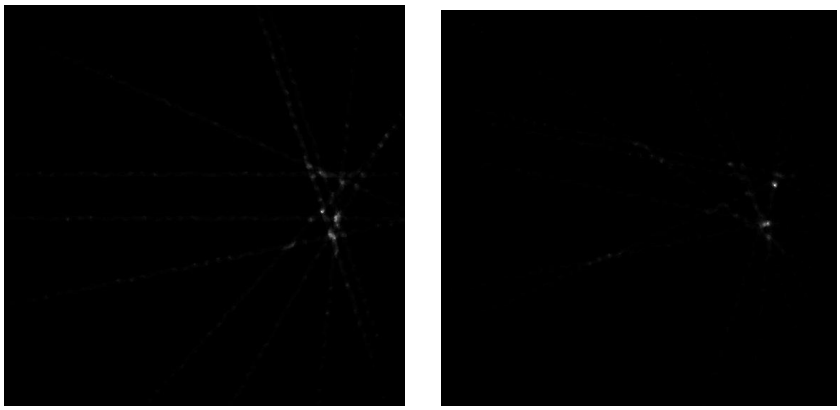

Figure 30: Images reconstructed with energy 1636keV. Images on the left were acquired with 52 rotations; images on the right were acquired with 56 rotations.

3.3.2 100,000 neutron histories

The simulations in the following section were run using 100,000 neutron histories.

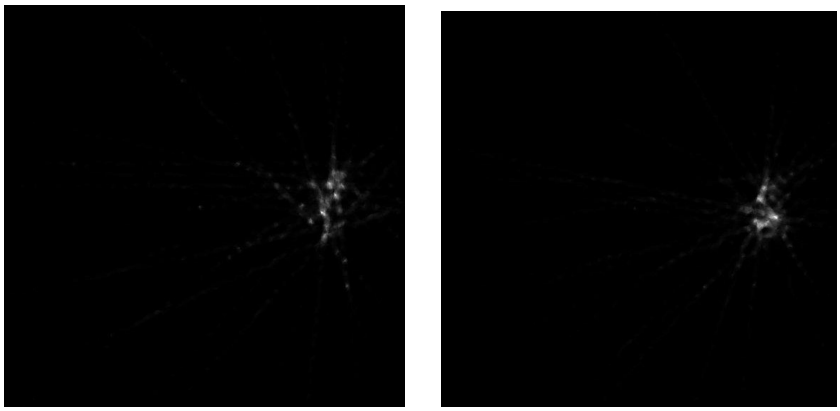

Figure 31: Images reconstructed with energy 440keV. Images on the left were acquired with 52 rotations; images on the right were acquired with 56 rotations.

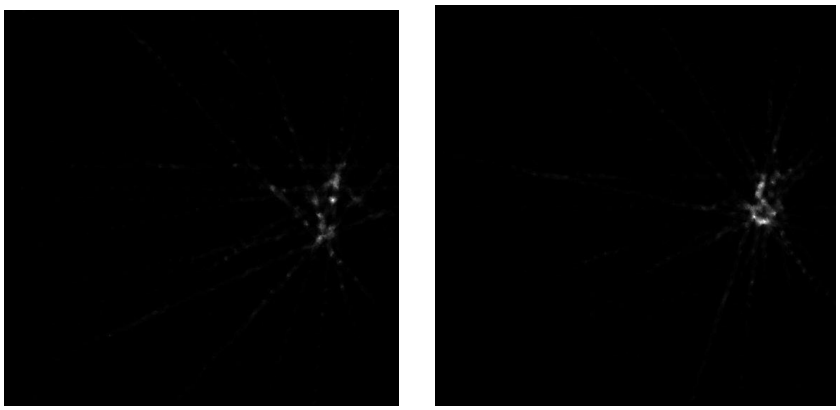

Figure 32: Images reconstructed with energy 1636keV. Images on the left were acquired with 52 rotations; images on the right were acquired with 56 rotations.

3.3.3 150,000 neutron histories

The simulations in the following section were run using 150,000 neutron histories.

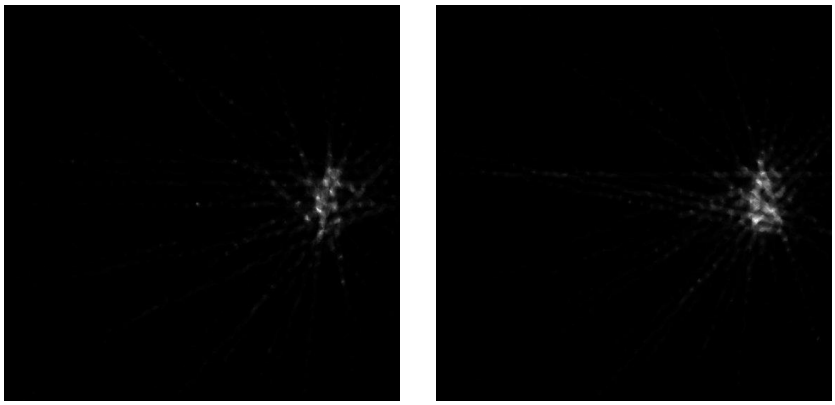

Figure 33: Images reconstructed with energy 440keV. Images on the left were acquired with 52 rotations; images on the right were acquired with 56 rotations.

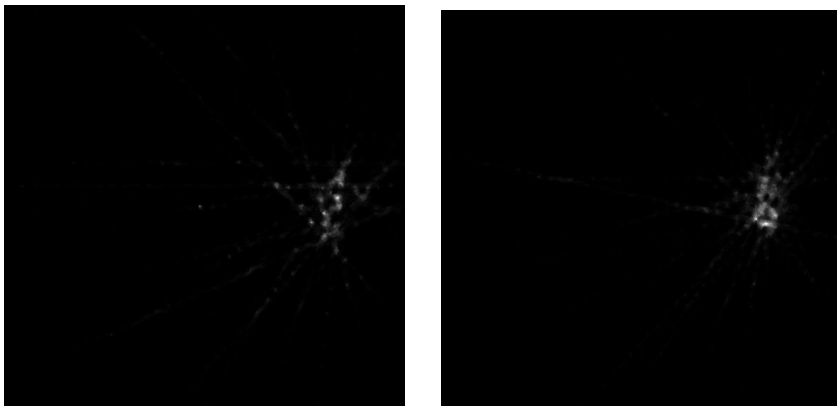

Figure 34: Images reconstructed with energy 1636keV. Images on the left were acquired with 52 rotations; images on the right were acquired with 56 rotations.

3.3.4 200,000 neutron histories

The simulations in the following section were run using 200,000 neutron histories.

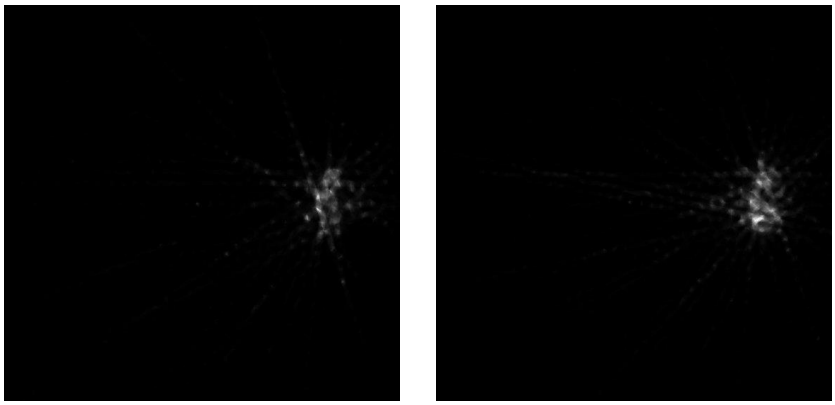

Figure 35: Images reconstructed with energy 440keV. Images on the left were acquired with 52 rotations; images on the right were acquired with 56 rotations.

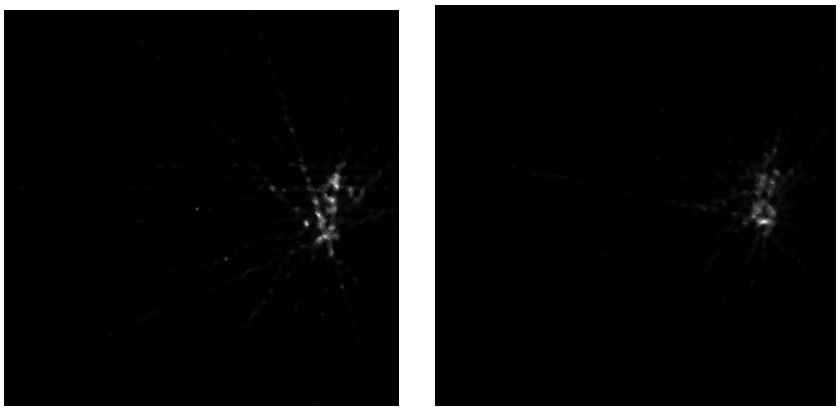

Figure 36: Images reconstructed with energy 1636keV. Images on the left were acquired with 52 rotations; images on the right were acquired with 56 rotations.

4. Image Analysis and Comparison

The images above were categorized into three sets for comparison,

1). From simulations by 50,000 neutron histories: 5MeV, 3.2MeV, 2.5MeV;

2). From simulations of the 3.2MeV source: 50,000 neutron histories, 100,000 neutron histories, 150,000 neutron histories, 200,000 neutron histories;

3). From simulations of 2.5MeV source: 50,000 neutron histories, 100,000 neutron histories, 150,000 neutron histories, 200,000 neutron histories;

Image parameters were compared among the images in each comparison set, i.e. average intensity, and the differences between the sizes of the reconstructed tumor described by FWHM and the actual tumor, which was measured to be 77.25mm*22.65mm in the previous section.

4.1 Comparison 1

Table 2 is the result of comparison between 50,000-neutron-history images reconstructed with different energies of three source beams of 5MeV, 3.2MeV and 2.5MeV acquired by 52 phantom translations, and table 3 is the result of comparing images obtained by 56 translations. The number of neutron histories run for these simulations was 50,000.

From the tables below, it can be seen that as the energy of the neutron source was decreased, the tumor region on the image became darker making it more difficult to distinguish tumor from the surrounding environment. But the smaller standard

deviations indicate that the tumor region is more focused with a lower-energy source, which gives a more confident tumor location on the reconstructed images. The size of tumor is generally underestimated compared to the actual tumor size on all the reconstructed images, of which those simulated with 5MeV neutrons appear to show the malignant area of a closest size to that of the real one than 3.2MeV and 2.5MeV neutrons.

Table 2: Comparison between 52-translation images of 5MeV, 3.2MeV and 2.5MeV.

Source energy (MeV)	Reconstruction energy (keV)	Average intensity of tumor region on the reconstructed image	Fractional standard deviation of reconstructed image intensity	Reconstructed tumor size (FWHM/mm*mm)	Difference from the actual tumor size
5	440	66.402	0.6475	48.15*13.06	37.67%*42.34%
	1636	75.091	0.5997	40.12*13.06	48.06%*42.34%
	2313	68.960	0.5860	45,17*18.81	41.53%*16.95%
	4439	94.659	0.6016	71.54*32.5	7.39%*43.49%
3.2	440	50.339	0.6902	8.09*7.83	89.53%*65.43%
	1038	35.548	0.7416	4.21*5.49	94.55%*75.76%
	1636	47.391	0.8339	7.13*7.66	90.77%*66.18%
	2313	37.284	0.9514	5.5*5.48	92.88%*75.81%
	2391	48.452	0.8027	6.32*5.54	91.82%*75.54%

2.5	440	34.620	1.0170	5.34*5.6	93.09%*75.28%
	1636	15.772	1.6021	2.53*2.95	96.72%*86.98%

Table 3: Comparison between 56-translation images of 5MeV, 3.2MeV and 2.5MeV.

Source energy (MeV)	Reconstruction energy (keV)	Average intensity of tumor region on the reconstructed image	Fractional standard deviation of reconstructed image intensity	Reconstructed tumor size (FWHM/mm*mm)	Difference from the actual tumor size
5	440	66.906	0.5804	42.4*36.13	45.11%*59.51%
	1636	91.502	0.4094	67.28*24.25	12.91%*7.06%
	2313	83.183	0.5585	55.51*19.25	28.14*%13.48%
	4439	115.095	0.4829	69.84*25.91	9.59%*16.45%
3.2	440	42.030	0.7652	6.82*7.75	91.17%*65.78%
	1038	42.177	1.0450	4.84*29.5	93.73%*30.24%
	1636	40.575	1.0032	34.85*22.59	54.89%*0.26%
	2313	45.334	0.9033	13.98*9.79	81.90%*56.78%
	2391	28.286	1.2588	40.20*5.14	47.96%*77.32%
2.5	440	23.739	1.4268	6.19*8.46	91.99%*62.65%
	1636	27.589	1.3212	2.83*3.42	96.34%*84.90%

4.2 Comparison 2

In order to see how the number of neutrons changes the tumor representation on the reconstructed images, simulations were set up with 50,000, 100,000, 150,000 and 200,000 3.2MeV neutron events.

By comparing the parameters listed in table 4 and table 5, increasing the number of neutron histories has a positive influence on the accuracy of tumor size estimation. And more incident neutrons could improve the brightness of the tumor, however, degrade the tumor concentration on the image.

Table 4: Comparison between 52-translation images of 3.2MeV simulated with 50,000, 100,000, 150,000 and 200,000 neutron histories.

Number of neutron histories	Reconstruction energy (keV)	Average intensity of tumor region on the reconstructed image	Fractional standard deviation of reconstructed image intensity	Reconstructed tumor size (FWHM/mm* mm)	Difference from the actual tumor size
50,000	440	50.339	0.6902	8.09*7.83	89.53%*65.43%
	1038	35.548	0.7416	4.21*5.49	94.55%*75.76%
	1636	47.391	0.8339	7.13*7.66	90.77%*66.18%
	2313	37.284	0.9514	5.5*5.48	92.88%*75.81%
	2391	48.452	0.8027	6.32*5.54	91.82%*75.54%
100,000	440	67.934	0.6420	59.6*11.28	22.85%*50.20%
	1038	35.919	0.9043	55.74*8.2	27.84%*63.8%

	1636	38.981	0.8924	14.71*6.98	80.96%*69.18%
	2313	41.366	0.8716	29.92*7.39	61.27%*67.37%
	2391	24.415	1.2278	6.61*9	91.44%*60.26%
150,000	440	76.152	0.6529	67.57*41.15	12.53%*81.68%
	1038	54.666	0.8675	34.5*17.27	55.34%*23.75%
	1636	47.399	0.7307	9.85*7.96	87.27%*64.86%
	2313	52.160	0.7726	52.5*33.27	32.04%*46.89%
	2391	38.908	0.9230	74.98*14.31	2.94%*36.82%
200,000	440	89.132	0.4700	67.88*29.49	12.13%*30.20%
	1038	63.499	0.6560	33.14*8.15	57.10%*64.02%
	1636	50.841	0.6343	59.48*8.21	23.00%*63.75%
	2313	57.045	0.6712	59.94*20.26	22.41%*10.55%
	2391	43.342	1.0034	74.26*12.28	3.87%*45.78%

Table 5: Comparison between 56-translation images of 3.2MeV simulated with 50,000, 100,000, 150,000 and 200,000 neutron histories.

Number of neutron histories	Reconstruction energy (keV)	Average intensity of tumor region on the reconstructed image	Fractional standard deviation of reconstructed image intensity	Reconstructed tumor size (FWHM/mm*mm)	Difference from the actual tumor size
50,000	440	42.030	0.7652	6.82*7.75	91.17%*65.78%

	1038	42.177	1.0450	4.84*29.5	93.73%*30.24%
	1636	40.575	1.0032	34.85*22.59	54.89%*0.26%
	2313	45.334	0.9033	13.98*9.79	81.90%*56.78%
	2391	28.286	1.2588	40.20*5.14	47.96%*77.32%
100,000	440	69.781	0.5899	48.4*17.79	37.35%*21.46%
	1038	35.306	1.0244	42.52*12	44.96%*49.02%
	1636	69.781	0.5899	28.16*37.78	63.55%*66.80
	2313	51.254	0.7940	34.73*7.36	55.04%*67.51%
	2391	37.528	0.9914	8.27*19.4	76.35%*14.04%
150,000	440	63.507	0.6504	65.99*19.75	14.58%*12.80%
	1038	53.829	0.8483	56.85*23.31	26.41%*2.91%
	1636	48.297	0.6764	39.03*19.11	49.48%*15.63%
	2313	63.118	0.7210	47.83*27.14	38.08%*19.82%
	2391	46.024	0.8466	43.69*30.11	43.44%*32.94
200,000	440	71.140	0.6610	61.7*25.21	20.13%*11.3%
	1038	47.441	0.7295	33.52*8.02	56.61%*64.59%
	1636	47.391	0.7992	58.18*21.35	24.69%*5.74%
	2313	65.706	0.6962	39.96*26.94	48.27%*15.92
	2391	43.491	0.7506	7.47*6.45	90.33%*71.52%

4.3 Comparison 3

A similar comparison to the one described in section 4.2 was done with a 2.5 MeV neutron source and the results basically remain constant with comparison 2. It is certain that a larger number of neutrons will contribute to a brighter tumor region in the image. The difference from 2.5MeV source case is that images obtained from running 100,000 neutron events gave the most precise tumor size on the scanned coronal plane.

Table 6: Comparison between 52-translation images of 2.5MeV simulated with 50,000, 100,000, 150,000 and 200,000 neutron histories.

Number of neutron histories	Reconstruction energy (keV)	Average intensity of tumor region on the reconstructed image	Fractional standard deviation of reconstructed image intensity	Reconstructed tumor size (FWHM/mm* mm)	Difference from the actual tumor size
50,000	440	34.620	1.0170	5.34*15.54	93.09%*31.39%
	1636	15.772	1.6021	2.53*2.95	96.72%*86.98%
100,000	440	42.206	0.7924	74.73*12.74	3.26%*43.75%
	1636	32.813	0.9480	75.68*5.46	2.03%*75.89%
150,000	440	50.905	0.6835	53.42*24.92	30.85%*10.02%
	1636	37.557	0.8354	41.65*7.16	46.08%*68.39%
200,000	440	50.143	0.6206	51.32*10.26	33.57%*54.7%
	1636	47.187	0.8522	71.1*15.09	7.96%*33.38%

Table 7: Comparison between 56-translation images of 2.5MeV simulated with 50,000, 100,000, 150,000 and 200,000 neutron histories.

Number of neutron histories	Reconstruction energy (keV)	Average intensity of tumor region on the reconstructed image	Fractional standard deviation of reconstructed image intensity	Reconstructed tumor size (FWHM/mm* mm)	Difference from the actual tumor size
50,000	440	23.739	1.4268	6.19*8.46	91.99%*62.65%
	1636	27.589	1.3212	2.83*3.42	96.34%*84.90%
100,000	440	40.352	0.9298	58.3*35.1	24.53%*54.97%
	1636	60.354	0.7466	58*34*4.84	24.48%*78.63%
150,000	440	69.309	0.6205	46.34*9.56	40.01%*57.79%
	1636	51.115	0.7480	68.61*17.15	11.18%*24.28%
200,000	440	53.172	0.7452	59.82*15.38	22.56%*32.10%
	1636	48.243	0.7171	47.45*14.18	38.58%*37.40%

5. Discussion

Results of the above comparisons reveal that as the source energy decreases, the tumor representation in the reconstructed image is affected on the following aspects. The brightness of tumor is compromised because even though the neutron interaction cross-section increases as the neutron energy decreases, the neutron inelastic scattering cross-section could decrease which contributes mainly to NSECT imaging. Nevertheless, fewer gammas detected will degrade the accuracy of estimating the size of tumor area determined by the difference of malignancy sizes between in the reconstructed images and in the actual phantom.

In order to compensate the loss on the tumor representing performance of NSECT by lower-energy source, different numbers of neutron histories were tried in the simulations. The positive effect that more neutrons have on the tumor representation can be seen obviously on the reconstructed image. The tumor region becomes brighter and easier to be distinguished, and the estimation on tumor size is closer to the real size.

Consider the images reconstructed with 440keV(Na) for example. The one generated with the 5MeV neutron source estimated the size of tumor region with an error of around 40% to 50% on two dimensions, as the energy of neutrons decreased to 3.2MeV, the error increased to about 80%, and it gets larger (90%) in images acquired by 2.5MeV neutrons. The reconstructed images involve much more noise demonstrated by the fractional standard deviations with lower-energy neutrons. But from the above data,

the noises in the reconstructed tumor, as well as the degradation in detection accuracy, i.e. the precise estimation on the size of tumor area, can be reduced by an increasing number of source particles. In section 4.2 and 4.3, the estimation error was on the decline with more incident neutrons. As for images of 3.2MeV source, the error dropped to the same level as in images of 5MeV source when the incident neutron number increased to 100,000 and it can even decrease to 10% to 20% with four times number of incident neutrons (200,000). In 2.5MeV source case, 100,000 neutrons, 150,000 neutrons and 200,000 neutrons could generate improved-quality images with more accurate tumor size as well. In this project, we've only tested setting 52 and 56 phantom translations, 56-translational images provided a slightly closer tumor size to the actual one but further investigation is needed for a solid conclusion.

The effect of lower-energy source neutrons discovered in the present work is of significant clinical relevance because it is preferred to tackle a diagnosis task in clinics with neutron source of lower energy out of some realistic concerns. Except for the advantage on smaller dose delivered to patients, neutrons of lower-energy can be produced in a compact neutron generator, such as DD neutron generator. Thus, more options of neutron source are potentially feasible for a NSECT application, which is a great encouragement for developing NSECT into a clinically cost-effective imaging technique in the future.

6. Conclusion and Future Work

The result of this work demonstrates the relationship between the energy of the neutron source and the ability of representing tumor on a NSECT image. The neutron source of lower energy could cause loss in the accuracy of tumor detection and underestimation of the tumor size, which can be compromised by an increase on the number of incident neutrons. In concrete terms, for an image of the same quality as 5MeV neutron source offered, at least twice number of incident neutrons of lower-energy (2.5MeV or 3.2MeV) is required. This conclusion allows more options as NSECT source generator and has a profound impact on its clinical usage. For example, DD generator energies were not considered suitable for NSECT imaging because of their inability to excite high-energy nuclear isotopes. However, based on the results demonstrated in this work, low-energy neutrons from DD generators can be sufficient for NSECT imaging, which makes DD generators a feasible neutron source in NSECT.

There are also limitations in this evaluation study. All the simulations were run with a phantom tumor of the same elemental composition as the cancerous tissue in human breast and the tumor was surrounded by vacuum environment. But in a real clinical case, the tumor is supposed to be located in the patient body. The nuclei in the neighboring normal breast can interact with incident neutrons and affect the acquired images. Future work is encouraged to do using a more realistic phantom including the tumor situating in human body. Another factor that makes the conclusion of this study

less firm is that the contouring of cancerous region on the images during analysis process and the measurement of FWHM were accomplished manually, so the results could be affected by subjective judgments. It is suggested for the future study on this topic to measure the FWHM at several different places on the contoured tumor region and take the average value for a more reasonable estimation.

In summary, this work has demonstrated the potential of the NSECT imaging system being implemented as a clinical application for the viability of using a low-energy neutron source but more investigations are to be done to improve its diagnostic ability before performing imaging in a hospital.

References

Agostinelli, S., Allison, J., Amako, K. A., Apostolakis, J., Araujo, H., Arce, P., ... & Behner, F. (2003). *GEANT4—a simulation toolkit*. Nuclear instruments and methods in physics research section A: Accelerators, Spectrometers, Detectors and Associated Equipment, *506*(3), 250-303.

Bender JE, Kapadia AJ, Sharma AC, Tourassi GD, Harrawood BP, Floyd CE. *Breast cancer detection using neutron stimulated emission computed tomography: Prominent elements and dose requirements.* Med. Phys. 34 3866–3871, 2007

Floyd CE Jr, Howell C, Harrawood BP, Crowell A, Kapadia AK, Macri R, Xia J, Pedroni R, Bowsher JE, Kiser M, Tourassia GD, Tornow W, Walter R. *Neutron stimulated emission computed tomography of stable isotopes.* Proc. SPIE 5368 248–254, 2004

Floyd CE Jr, Bender JE, Sharma AC, Kapadia AJ, Xia J, Harrawood BP, Tourassi GD, Lo JY, Crowell A, Howell CR. *Introduction to neutron stimulated emission computed tomography.* Phys. Med. Biol. 51 3375-3390, 2006

Fong, G. (2016). *Collimation of a D-D neutron generator for clinical implementation of neutron stimulated emission computed tomography: A monte carlo study* (Master's thesis). Retrieved from ProQuest Dissertations & Theses Global. (1795570286).

Kapadia AJ, Sharma AC, Bender JE, Tourassi GD, Howell CR, Crowell AS, Kiser MR, Harrawood BP, Floyd CE. *Neutron stimulated emission computed tomography for diagnosis of breast cancer.* IEEE Trans. Nucl. Sci. 55 501–509, 2008a

Raterman, G. M. (2013). *Neutron Stimulated Emission Computed Tomography: Optimization of Acquisition* (Master's thesis, Duke University).

RADIA, I., & REP, Y. Neutron Generators for Analytical Purposes.

Silva MP, Soave DF, Ribeiro-Silva A, Poletti ME.*Trace elements as tumor biomarkers and prognostic factors in breast cancer: a study through energy dispersive x-ray fluorescence*. BMC Research Notes, *5*(1), 194. doi:10.1186/1756-0500-5-194

Segars, W. P., Sturgeon, G., Mendonca, S., Grimes, J., & Tsui, B. M. W. (2010). *4D XCAT phantom for multimodality imaging research*. Medical Physics, *37*(9), 4902–4915.